HHS Public Access

Author manuscript

Toxicol Appl Pharmacol. Author manuscript; available in PMC 2017 November 01.

Published in final edited form as:

Toxicol Appl Pharmacol. 2016 November 01; 310: 129–139. doi:10.1016/j.taap.2016.09.011.

A MOUSE MODEL OF ALCOHOLIC LIVER FIBROSIS-ASSOCIATED ACUTE KIDNEY INJURY IDENTIFIES KEY MOLECULAR PATHWAYS

Shinji Furuya[1], **Grace A. Chappell**[1], **Yasuhiro Iwata**[1], **Takeki Uehara**[2], **Yuki Kato**[2], **Hiroshi Kono**[3], **Ramon Bataller**[4], and **Ivan Rusyn**[1,*]

[1]Department of Veterinary Integrative Biosciences, Texas A&M University, College Station, TX, USA

[2]Laboratory of Veterinary Pathology, Osaka Prefecture University, Osaka, Japan

[3]First Department of Surgery, University of Yamanashi, Yamanashi, Japan

[4]Division of Gastroenterology & Hepatology, Department of Medicine, University of North Carolina, Chapel Hill, NC, USA

Abstract

Clinical data strongly indicate that acute kidney injury (AKI) is a critical complication in alcoholic hepatitis, an acute-on-chronic form of liver failure in patients with advanced alcoholic fibrosis. Development of targeted therapies for AKI in this setting is hampered by the lack of an animal model. To enable research into molecular drivers and novel therapies for fibrosis- and alcohol-associated AKI, we aimed to combine carbon tetrachloride (CCl_4)-induced fibrosis with chronic intra-gastric alcohol feeding. Male C57BL/6J mice were administered a low dose of CCl_4 (0.2 ml/kg 2×wk/6wks) followed by alcohol intragastrically (up to 25 g/kg/day for 3wks) and with continued CCl_4. We observed that combined treatment with CCl_4 and alcohol resulted in severe liver injury, more pronounced than using each treatment alone. Importantly, severe kidney injury was evident only in the combined treatment group. This mouse model reproduced distinct pathological features consistent with AKI in human alcoholic hepatitis. Transcriptomic analysis of kidneys revealed profound effects in the combined treatment group, with enrichment for 53 damage-associated pathways, such as apoptosis, inflammation, immune-response and hypoxia. Interestingly, *Harcr1* and *Lcn2*, biomarkers of AKI, were markedly up-regulated. Overall, this study established a novel mouse model of fibrosis- and alcohol-associated AKI and identified key mechanistic pathways.

Introduction

Alcohol's impact on kidney function is complex, with some reports of moderate consumption being beneficial in chronic nephropathy (Schaeffner and Ritz, 2012). Upon oral

*Correspondence to: Ivan Rusyn, Department of Veterinary Integrative Biosciences, Texas A&M University, College Station, TX 77843-4458, USA. irusyn@tamu.edu.

Disclosure

The authors have no conflicts to disclose.

ingestion, alcohol is diffusing readily through cell membranes and is metabolized by most tissues to acetaldehyde, a highly reactive electrophile (Zakhari, 2006). Alcohol toxicity is also associated with formation of reactive oxygen and nitrogen species, depletion of co-factors (*e.g.*, NAD+), impairment in energy homeostasis and activation of pro-inflammatory and other signaling pathways in many organs (Rusyn and Bataller, 2013). Liver is one of the major targets for alcohol with disease severity ranging from steatosis to steatohepatitis, cirrhosis, and hepatocellular carcinoma. Other tissues are also impaired by chronic alcohol abuse, including acute and chronic kidney disease (Schaeffner and Ritz, 2012).

Alcohol abuse causes half of the cases of cirrhosis worldwide (World Health Organization, 2014). Patients with alcoholic cirrhosis often develop alcoholic hepatitis, an acute-on-chronic form of liver injury that carries a high mortality rate. In these patients, short-term mortality is heavily influenced by early occurrence of acute kidney injury (AKI) (Altamirano *et al.*, 2012). Alcoholic hepatitis is an acute-on-chronic disease (Casanova and Bataller, 2014) characterized by high mortality due to multiple organ failure and systemic inflammatory response syndrome even in the absence of an infection (Michelena *et al.*, 2015). Because of the shortage of effective treatment options for alcoholic hepatitis to supplement non-specific first-line therapy with prednisolone or pentoxifylline, there is a need to identify key pathogenic drivers of this disease, including impaired kidney function, through development of rodent models (Casanova and Bataller, 2014).

There is little information in the published literature regarding the impact of alcohol on kidney function and pathology from rodent models. On the one hand, mild nephropathy has been observed in rats fed alcohol-containing liquid diet for either 6 or 4 weeks (Van Thiel *et al.*, 1977; Latchoumycandane *et al.*, 2014). However, no effect on kidney function or kidney injury has been reported in previous mouse studies, including the protocols where large amounts of alcohol are administered, either through intragastric feeding (Kono *et al.*, 2000; Ueno *et al.*, 2012), or in a liquid diet followed by alcohol binge (Bertola *et al.*, 2013). On the other hand, liver fibrosis and neutrophil infiltration, together with bilirubinostasis and presence of megamitochondria, are main pathological diagnoses strongly predictive of mortality from alcoholic hepatitis (Altamirano *et al.*, 2014). Even though several experimental models of alcoholic steatohepatitis in mice are available (Ueno *et al.*, 2012; Bertola *et al.*, 2013), none reproduces these features of severe alcoholic hepatitis. Interestingly, recent mouse studies demonstrated that co-administration of pro-fibrogenic stimulus carbon tetrachloride (CCl_4) (Chiang *et al.*, 2013), or pro-inflammatory factor lipopolysaccharide (Affo *et al.*, 2014) with moderate alcohol consumption through a liquid diet results in exacerbation of liver injury through both activation of the hepatic stellate cells and inflammatory cascades.

Because alcoholic hepatitis is a severe form of alcohol-associated disease in subjects with pre-existing liver pathologies such as fibrosis, we aimed to replicate the acute-on-chronic nature of this life-threatening human syndrome in a mouse model. Specifically, we tested a hypothesis that alcohol toxicity will be exacerbated in pro-fibrotic conditions in both liver and kidney. In contrast to other models, we elicited fibrosis through sub-chronic (6 weeks) low-dose treatment with CCl_4 followed by intragastric alcohol feeding with or without

additional continuous administration of one-half dose of CCl_4 for 3 weeks. This design resulted in a clinical phenotype of alcoholic hepatitis complicated by acute kidney injury.

Materials and Methods

Animals

Male mice (C57BL/6J, 20–25 g, 12 weeks of age) were obtained from the Jackson Laboratories (Bar Harbor, ME) and housed in a clean, temperature-controlled environment with a 12-h light-dark cycle and were given free access to regular laboratory chow diet and water for housing in regular cages. All animals were given humane care in compliance with National Institutes of Health guidelines and severe alcohol intoxication was assessed carefully to evaluate the development of tolerance using a 0–3 behavioral scoring system (0=normal behavior, 1=sluggish movement, 2=loss of movement, but animal moves when stimulated, 3=loss of consciousness). This work was approved by the Institutional Animal Care and Use Committee at UNC-Chapel Hill.

Diets and Treatment

CCl_4 (>99.5% pure) and olive oil vehicle were from Sigma (St. Louis, MO), ethyl alcohol (190 proof, Koptec) was from VWR (Radnor, PA). Procedures for CCl4 injections were as detailed elsewhere (Uehara *et al.*, 2014). Prior to each injection, 1 ml of pure CCl_4 was dissolved in olive oil to a final volume of 10 ml (0.01%, v/v) and stored in light-protected bottle. Mice were intraperitoneally injected (15 ml/kg) with dissolved CCl_4 (0.2 ml/kg) diluted in olive oil vehicle or only olive oil vehicle twice a week for 6 weeks, starting on day 1 of the experiment (Supplemental Figure 1, injections performed on Monday and Thursday at 9 am). Mice were maintained on normal animal chow with free access to food/water for this duration. After 6 weeks of treatment, animals underwent surgical intragastric intubation (Kono *et al.*, 2000). Following surgery, mice were housed in individual metabolic cages and allowed one week to recover with ad libitum access to food and water. Animals had free access to water and non-nutritious cellulose pellets throughout the study. Alcohol groups received high-fat diet containing ethyl alcohol as detailed elsewhere (Kono *et al.*, 2000). Alcohol was delivered continuously through the intragastric cannula initially at 16 g/kg/day and was gradually increased 1 g/kg every 2 days until day 14. The dose was then increased by 1 g/kg every 3 days until the dose reached 25 g/kg/day.

Five experimental groups (n=3–4 per group) comprised this study. Control (“Cont”) group are animals that received i.p. injections (2x week) of olive oil vehicle for 6 weeks. “CCl_4(6w)” group are animals that received i.p. injections (2x week) of CCl_4 (0.2 ml/kg) for 6 weeks. “CCl_4(9w)” are animals that received i.p. injections (2x week) of CCl_4 (0.2 ml/kg) for 6 weeks and then received i.p. injections (2x week) of CCl_4 (0.1 ml/kg) for 3 weeks. “EtOH” group are animals that received i.p. injections (2x week) of olive oil vehicle for 6 weeks and then were administered alcohol intragastrically for 3 weeks. “CCl_4(9w)+EtOH” group are animals that received i.p. injections (2x week) of CCl_4 (0.2 ml/kg) for 6 weeks and then were administered alcohol intragastrically with continuous i.p. injections (2x week) with CCl_4 (0.1 ml/kg).

Sample Collection

Blood was collected at sacrifice from *vena cava* into heparin tubes and serum was isolated. Sections of the median, left lateral liver lobes and kidney were fixed in 10% formalin and embedded in paraffin and the remaining tissues were frozen and stored at −80°C. Urine was collected using metabolic cage every morning after starting alcohol administration (at 9 am) and stored at −20°C until assayed. Ethanol concentration was determined by measuring absorbance at 366 nm resulting from the reduction of NAD+ to NADH by alcohol dehydrogenase as detailed elsewhere (Bergmeyer, 1988).

Liver and kidney histopathological evaluation

Formalin-fixed/paraffin-embedded liver and kidney sections were stained with hematoxylin/eosin (H&E). Liver and kidney pathology was evaluated in a blind manner by two certified veterinary pathologists. For quantitative analysis of liver injury, assessments were noted for each liver sample; in addition, lesions of interest were semi quantitatively as follows. Mallory-Denk bodies (MDBs) and ductular reaction were both scored as 0–4 (0, none; 1, rare; 2, moderate; 3, frequent; 4, abundant). MDB scoring was done for zone 1 or zones 1 plus 3 because MDBs are found preferentially in zone 1 in cholestasis and copper storage liver diseases. Hepatocyte ballooning was scored as 0–3 (0, none; 1, rare; 2, frequent; 3, abundant) and zonal location noted. Bile plugs and non-bile pigment deposition, and intraductal lithiasis were noted for location and semi quantified (0–3 and 0–4, respectively). Periductal fibrosis was scored as 0–1 (0, absent; 1, present). Steatosis was scored as 1–3 (1, <1%; 2, 1%–5%; 3, >5%).

For quantitative analysis of kidney injury in the form of dilatation and regeneration of the focal renal tubule lesions was scored as 0–4 (0, none; 1, minimal; 2, mild; 3, moderate; 4, marked). In addition, PAS (periodic acid–Schiff stain for proteinaceous material & basement membrane detection), DFS (direct first scarlet stain for amyloid detection) and PTAH (phosphotungstic acid hematoxylinstain stain for detection of fibrin) staining was performed using established protocols. To determine the presence of fibrosis in liver and kidney, liver and kidney sections were subjected to alpha-smooth muscle actin (α-SMA) immunohistochemistry, Masson's trichrome and Sirius red staining. At least five fields from all animals of each group were analyzed.

Immunohistochemistry

Paraffin-embedded liver sections (5 μm thick) were stained with primary antibodies using Dako Antibody Dilution solution (Dako, Carpinteria, CA). The primary antibodies used in these experiments were: rabbit anti-4-hydroxynonenal (4-HNE; Alpha Diagnostics, San Antonio, TX; 1:1000, 60 min, room temperature), mouse anti-human alpha-smooth muscle actin (αSma; abcam, Cambridge, MA; 1:200, 10 min, room temperature), goat anti-mouse TIM-1/KIM-1/HAVCR (R&D systems, Minneapolis, MN; 2 mm/ml, 10 min, room temperature), and rat anti-mouse CD68 (CD68; AbD serotec, Raleigh, NC; 1:200, overnight, 4°C). We used Dako EnVision System (Dako, Carpinteria, CA) HRP kit for HNE and αSma, Goat IgG HRP-conjugated antibody (R&D systems, Minneapolis, MN; 1:100, 10min, room temperature) as secondary antibody for KIM-1, and VECTASTAIN ABC Kit (Rat; Vector, Burlingame, CA) for CD68. Dako Liquid DAB+ Substrate chromogen System (Dako,

Carpinteria, CA) was employed for visualization. Slides were counterstained with filtered Mayer's hematoxylin (Sigma) for 5 min. Quantitative analysis was performed using Image-Pro Premier 9.1 (Media Cybernetics, Silver Spring, MD) at 100× magnification. For α-SMA and 4-HNE, five fields of Liver and Kidney tissue were randomly selected to calculate percent of positively stained area.

Biochemical Measurements

Serum creatinine levels were determined spectrophotometrically with the Creatinine (serum) Assay kits (Cayman Chemical, Ann Arbor, MI). Serum Urea (BUN) levels were determined spectrophotometrically with the QuantiChrom Urea Assay Kit (BioAssay Systems, Hayward, CA). Urine creatinine levels were determined fluorometrically with the Creatinine Assay kits (Sigma). Urine protein levels were quantified using the Qbit. Hepatic levels of methionine, SAM, SAH, homocysteine, and reduced (GSH) and oxidized (GSSG) glutathione were measured by HPLC coupled with coulometric electrochemical detection as previously described (Melnyk *et al.*, 1999).

RNA Isolation and Sequencing

Total RNA was extracted from liver using the RNeasy Mini kit (Qiagen, Valencia, CA) RNA concentrations were measured with NanoDrop ND-1000 spectrophotometer (NanoDrop Technologies, Wilmington, DE) and quality was verified using the Bio-Analyzer (Agilent Technologies, Santa Clara, CA). Libraries for RNA-seq were prepared using the Illumina TruSeq mRNA Sample Prep Kit (Illumina, San Diego, USA). Single-end (50bp) sequencing was carried out using the Illumina HiSeq 2500 platform. RNA-seq reads were aligned to appropriate reference genomes (NCBI mm9) using the "SNP-tolerant" GSNAP software. This alignment pipeline allows for the elimination of mapping biases that arise from discrepancies in genetic variation between individual samples and a standard reference genome, at both homozygous and heterozygous sites. Sequencing quality and mapping statistics were compared across all samples and duplicate entries and transcripts with less than 10 counts were removed. Genes which were differentially expressed in treated group relative to control mice were identified by a Wald test followed by Benjamini-Hochberg correction for multiple testing using the DESeq2 and TCC R packages. A q value <0.1 was used to define differentially expressed genes between each group. Gene expression data are available at GEO (GSE83529).

Pathway annotation of the differentially expressed genes

The GGRNA tool was used to identify hypoxia-associated transcripts (Naito and Bono, 2012).The DAVID tool (Dennis *et al.*, 2003) was utilized to execute GO enrichment, KEGG pathway analysis, annotation and analysis of related diseases on the DEGs. Benjamini method was used to conduct multiple testing correction, and $p<0.05$ was considered as the significantly enriched threshold.

Quantitative real-time PCR

Total RNA (2 μg) was reverse transcribed using random primers and the high capacity cDNA archive kit (Applied Biosystems, Foster City, CA). The following assays (Applied

Biosystems, Foster City, CA) were used for quantitative real-time Polymerase-Chain Reaction: *Hacvr1* (Kim-1, Mm00506686_m1), *Lcn2* (Mm01324470_m1), *Timp1* (Mm01341361_m1), *CD68* (Mm03047343_m1), and *Gusb* (Mm001197698_m1). Reactions were performed in a 96-well assay format using Roche 480 instrument (Roche Applied Science, Indianapolis, IN). $^{\Delta}$Ct values for all genes relative to the control gene *Gusb* were determined. The $^{\Delta\Delta}$Ct were calculated using treated group means relative to strain-matched control group means.

Western Blotting

Proteins were extracted from the liver and analyzed by Pierce BCA Protein Assay Kit (Thermo Fisher Scientific Inc, Waltham, MA). Primary antibodies against beta-actin and Cytochrome P450 2e1 (Cyp2e1) were from Abcam (Cambridge, MA). IRDye680-conjugated secondary antibodies were from LiCor (Lincoln, NE). Blots were scanned using the Odyssey system (LiCor) and intensity of the bands was quantified with Image Studio Ver4.0 (LiCor). The intensity of protein bands on the blots was normalized to beta-actin and to control samples.

Statistical analyses

Statistical significance was determined using GraphPad Prism5 (San Diego, CA). Quantitative values are expressed as mean±SD unless otherwise noted. Statistical significance was evaluated using one-way ANOVA within each time point followed by the Tukey's post hoc test. Statistical significance is indicated at any level below $p < 0.05$.

Results

Intragastric administration of alcohol does not induce significant kidney injury in mice

Intragastric feeding of high-fat diet containing alcohol is a well-established rodent model of alcohol toxicity (Kono *et al.*, 2000; Ueno *et al.*, 2012). Traditionally, histopathological and clinical chemistry assessment of the outcome of the studies that use this model focuses on the liver. Thus, we conducted detailed histopathological evaluation of the kidneys from two mouse studies where animals were administered alcohol (up to 27 mg/kg/d) in a high fat diet using an intragastric intubation model for 28 days. One study was conducted in male C57BL/6J mice (Powell *et al.*, 2010), and another was a study of inter-strain differences in alcohol-induced liver injury in male mice from 15 inbred strains (129S1/SvImJ, AKR/J, BALB/cJ, BALB/cByJ, BTBR T+tf/J, C3H/HeJ, C57BL/6J, C57BL/10J, DBA/2J, FVB/NJ, KK/HIJ, MOLF/EiJ, NZW/LacJ, PWD/PhJ, and WSB/EiJ) (Tsuchiya *et al.*, 2012). Between two studies, there were 53 mice that were administered high fat diet alone via intragastric cannula for 28 days and 72 animals that were co-administered alcohol in the same diet. Endpoints examined were light microscopy of H&E-stained slides, as well as specialized stains for proteinaceous material and basement membrane material (PAS stain), collagen (Masson's trichrome [MT] stain), amyloid (DFS stain), and fibrin (PTAH stain). Even though no evidence of kidney injury was observed in either alcohol- or high fat diet-fed animals using conventional light microscopy, we found hyaline-like material in the mesangial area in glomeruli in some animals. The material in the mesangial area was PAS-stain positive and MT-, PTAH-, DFS-stain negative (Figure 1). These lesions were classified

as hyaline glomerulopathy, a mild form of acute glomerulonephritis, with incidence of 21% (11 out of 53) in high fat diet-fed animals and 13% (9 out of 72) in alcohol and high fat diet-fed animals. No strain differences were observed in the incidence of the lesions and these data show that intragastric alcohol feeding for up to 28 days does not result in microscopically discernable kidney injury.

Alcohol intake induces kidney injury in mice with liver fibrosis

Next, we examined the effects of CCl_4, alcohol, or a combination treatment on liver and kidney phenotypes in mice. Characteristic cycling of circulating alcohol (French, 2005) was unaffected by co-administration of CCl_4 (Figure 2A, mean urine alcohol concentrations over last two weeks of intragastric feeding were EtOH=165±80 mg/dL and CCl_4(9w) +EtOH=163±87 mg/dL). Similarly, behavioral assessment of the degree of alcohol-associated inebriation of the animals in this study showed no differences among the groups (Figure 2B).

Continuous treatment with CCl_4 alone resulted in progressive liver injury, primarily characterized by fibrotic and inflammatory changes (Figure 3, Supplemental Figure 2), but no necrosis or elevation in serum enzymes (data not shown). Alcohol treatment for 4 weeks through an intragastric cannula resulted in liver enlargement and severe steatosis, with signs of inflammation and necrosis; however, combined treatment with both alcohol and CCl_4 markedly exacerbated liver injury and fibrosis (Supplemental Figure 2). Both lipid peroxidation and inflammatory cell infiltration were much more pronounced in the combined treatment group as compared to alcohol-only group, or to animals treated with CCl_4.

The effects of either treatment alone, or combination thereof, on kidney in this model were most relevant to the AKI phenotype in human alcoholic hepatitis. Neither CCl_4, nor alcohol treatments in isolation had an effect on the kidney pathology (Figures 4 and 5). In stark contrast, combined treatment resulted in about 20% increase in relative kidney weight, severe kidney injury and disruption of kidney function (Figures 4 and 5). Not only there were signs of severe capsule fibrosis and amphophilic material deposition in the glomeruli, as well as dilation and signs of regenerative proliferation in the renal tubules, but also profound upregulation of expression of injury, fibrosis and inflammation markers *Kim-1*, *Timp-1*, *Lcn2* and *CD68* (Figure 6). The entire renal cortex was affected by the combined treatment with alcohol and CCl_4. Interestingly, damage in the renal tubules was much more pronounced than the effect on the glomeruli; most of the tubules were dilated and with signs of regeneration (Figure 5B).

Macrophages produce pro-fibrotic and pro-inflammatory factors that help in the maintenance of mesenchymal cells, thereby promoting fibrosis (Humphreys *et al.*, 2010). Likewise, oxidative stress is critical in the pathophysiology of kidney injury (Santos *et al.*, 2008) and lipid peroxidation is a hallmark of oxidative stress (Niki, 2008). Indeed, in a combined treatment group we observed profound effects on both lipid peroxidation and inflammatory cell infiltrates, most of the positive staining was primarily located in the renal cortex (Figures 4G and H). Hepatic glutathione depletion after chronic alcohol consumption, another biomarker of oxidative stress, occurs in experimental animals and in humans

(Lauterburg and Velez, 1988; Tsuchiya *et al.*, 2012), an effect that was observed in our study with respect to the levels of glutathione (GSH) and GSH/GSSG ratio in the liver, but to a much lesser degree in kidney and not in serum (Supplemental Figure 3). Interestingly, protein levels of Cyp2e1 were increased, as expected, in EtOH-only group in the liver, but not in kidney, but were significantly lower in a combined-treatment group (Figure 7), demonstrating that oxidative stress in the animals in a combined treatment group is unrelated to Cyp2e1 induction, a major source of oxidants in alcoholic liver disease (Bradford *et al.*, 2005).

Alterations of methionine metabolism have been suggested to play an important role in the pathogenesis of alcoholic liver disease (Lu *et al.*, 2002), but little is known about the effect of alcohol on this pathway in kidney. To determine what changes in methionine cycle metabolites are elicited by alcohol and/or CCl_4 in different tissues, concentrations of methionine, S-adenosyl-L-methionine (SAM), and S-adenosyl-L-homocysteine (SAH) were measured (Supplemental Figure 4). Alcohol-associated liver injury is significantly inversely correlated with SAM/SAH ratio (Tsuchiya *et al.*, 2012), and we observed that a decrease in SAM was the most pronounced effect in liver and serum in EtOH group, but it was not reduced in the combined treatment group. In kidneys, both CCl_4 and EtOH treatments, alone or in combination, had a significant effect on SAM and SAM/SAH ratio.

Transcriptome analysis identifies degerulated pathways in alcohol-induced kidney injury

To further elucidate the mechanisms of fibrosis- and alcohol-associated AKI, transcriptome analysis was performed on kidney tissues (Figure 8). We observed very few significant expression changes in the CCl_4-alone treatment group; 29 genes in CCl_4 (6w) treatment group and 4 genes in CCl_4 (9w) treatment group were affected and comprised no significantly enriched pathway (Figure 8A and Supplemental Tables 1 and 2). In EtOH treatment group, we found 729 significantly differentially expressed genes characteristic of the induction of cytochrome P450 and drug metabolism and downregulation of terpenoid backbone biosynthesis pathways (Figure 8C).

In contrast, profound effects on gene expression were found in the combined treatment group (*i.e.*, alcohol administration to mice with liver fibrosis), with almost 8,000 transcripts significantly different from control (Figure 8D, Supplemental Table 3). This transcriptional response included enrichment for 53 damage-associated pathways, including apoptosis, inflammation, and immune response (Figure 8G). Specifically, *Havcr1/Kim1* (hepatitis A virus cellular receptor 1/Kidney injury molecule-1) and *Lcn2/Ngal* (Lipocalin 2/Neutrophil gelatinase-associated lipocalin), known biomarkers of renal dysfunction (*Lcn2* specifically in patients with liver cirrhosis (Belcher *et al.*, 2014)), were among the top (in terms of both significance and fold change) differentially expressed transcripts in the kidneys of mice with AKI (Figure 5G). Interestingly, several inflammatory genes were differentially regulated in the kidneys from mice with alcoholic fibrosis (e.g. *Vcam1, Spp1* and *Cxcl1*). In addition, fatty acid metabolism pathways and PPAR signaling were markedly downregulated, findings that are concordant with the observations in human nephropathies of various etiology (Guan, 2004). Finally, relatively few significantly affected pathways overlapped between alcohol-treated and combined treatment groups. Only lysosomal protein expression was among the

up-regulated transcripts (Figure 8E), while all significant pathways affected by alcohol alone were also affected in the combined treatment group (Figure 8F).

Because clinical alcoholic hepato-renal syndrome is commonly attributed to hemodynamic changes, lower renal perfusion rates and tissue hypoxia we also examined changes in gene and protein expression of hypoxia-related genes. Specifically, we have examined “hypoxia”-related transcript changes in all animals using RNA-seq data. We have used GGRNA tool, a transcript-oriented search engine for genes and transcripts (Naito and Bono, 2012), to derive a list of transcripts that have been annotated as relating to hypoxia in the mouse (Figure 9A and Supplemental Table 4) and were expressed in the dataset. Also, we have queried a subset of these transcript, those that have been tagged for “kidney” (Figure 9B and Supplemental Table 4). In the CCl_4(9w)+EtOH group there were marked changes in expression of most of these transcripts, with a predominant effect being upregulation. Furthermore, we found that Hif1a protein is markedly increased in the CCl_4(9w)+EtOH group (Figure 9C). We also confirmed expression changes in mRNA of several Hif-related genes using RT-PCR (Figure 9D).

Discussion

Severe cases of alcoholic hepatitis are often associated with the development of type 1 hepatorenal syndrome leading to AKI (European Association for the Study of Liver, 2012; Egerod Israelsen *et al.*, 2015). Renal dysfunction usually develops secondary to a decrease in blood pressure as part of an inflammatory response caused by, among several possible etiological factors, severe alcoholic hepatitis (Salerno *et al.*, 2007). This phenotype, however, is unattainable in the traditional rodent models of alcohol-induced injury which prompted our effort to combine a pro-fibrogenic treatment with alcohol administration. While high necrogenic doses of CCl_4 are known to cause injury and fibrosis in liver (Weiler-Normann *et al.*, 2007), kidney (Ogawa *et al.*, 1992) and other tissues, we aimed to achieve chronic pro-fibrogenic disease state without overt necro-inflammation. Our previous mouse studies (Uehara *et al.*, 2013) showed that continuous administration of low dose CCl_4 results in pronounced liver fibrosis with mild to minimal signs of hepatotoxicity, but no pathological effects on other tissues including the kidney, a result that was supported by the transcriptomic analysis of the kidney samples which showed only several; dozen transcripts as differentially expressed by CCl_4 treatment alone.

Previous studies of intragastric feeding of alcohol in mice showed that diffuse peri-cellular liver fibrosis is achievable only under conditions of a combination of high-fat “Western diet” pretreatment followed by administration of up to 32 g/kg/day alcohol for over 8 weeks (Kisseleva *et al.*, 2012). This phenotype represents a pericellular/perisinusoidal pattern observed in human alcoholic fibrosis that is known to begin with the classic “chicken-wire” fibrosis and progresses to the portal tracts as bridging central-portal or portal-portal fibrosis (Sakhuja, 2014). In our study, a more traditional mouse intragastric feeding model (Kono *et al.*, 2000), alcohol alone showed little evidence of fibrogenesis; however, in combination with CCl_4–induced liver fibrosis alcohol exacerbates liver injury. One explanation for this is the role of inflammation and oxidative stress (Uehara *et al.*, 2013). Both CCl_4 and alcohol are known to promote these mechanisms (Cabre *et al.*, 2000). Peroxidation of lipids leads to

cell damage and byproducts of lipid peroxidation have been shown to promote fibrosis (Parola *et al.*, 1996). Other potential mechanisms by which CCl_4 potentiates alcohol-induced liver fibrosis include modulation of the adaptive and innate inflammatory responses, activation of stellate cells into myofibroblast-like cells, and promotion of dysbiosis and increased gut permeability (Gomez-Hurtado *et al.*, 2011).

The findings of severe AKI in this mouse model of fibrosis- and alcohol-associated liver injury is significant. The precise renal pathological features in patients with alcoholic hepatitis are largely unknown. Our previous clinical studies investigating the incidence and impact of AKI in patients with alcoholic hepatitis (Altamirano *et al.*, 2012; Michelena *et al.*, 2015) did not include renal histological data. The main reason for the lack of histological data on kidney injury in humans is that kidney biopsy is extremely dangerous in patients with alcoholic hepatitis, who are severely coagulopathic. In our clinical experience, even transjugular renal biopsy carries a mortality risk in this patient population.

Based on our clinical experience and studies in alcoholic cirrhosis, AKI could be mainly due to hepatorenal syndrome and/or acute tubular necrosis. Patients with advanced liver fibrosis are predisposed to AKI including hepato-renal syndrome, which markedly impairs survival (Martin-Llahi *et al.*, 2011). Importantly, alcohol abuse is the main etiology among cirrhotic patients with AKI (Garcia-Tsao *et al.*, 2008). In fact, AKI frequently develops in patients with alcoholic hepatitis, probably related to hemodynamic derangements associated with systemic inflammatory response (Altamirano *et al.*, 2012). Importantly, our findings in the mouse model, both clinical and molecular, point strongly to the major role for hepato-renal syndrome associated with kidney tissue hypoxia in alcohol- and fibrosis-associated AKI. Specifically, presence of both etiological factors for alcoholic hepatitis was necessary to elicit AKI in the mouse model, while either factor alone produced virtually no effect on the kidney. Therefore, we posit that this mouse model is a considerable step forward in identifying critical co-morbidity factors that are behind precipitous worsening of the prognosis in subjects with alcoholic hepatitis.

The molecular pathogenesis of AKI in the setting of advanced cirrhosis is largely unknown (Gines and Schrier, 2009). Renal hypoperfusion due to the activation of systemic vasoconstrictors occurs in many cases, and is associated with decreased intrarenal synthesis of vasodilators. Prolonged renal hypoperfusion can lead to acute tubular necrosis, especially in patients with alcoholic cirrhosis. The current therapy for AKI in cirrhosis consists of splanchnic vasoconstrictors (i.e., terlipressin) and plasma volume expansion with albumin. Unfortunately, this therapy fails in many patients and targeted therapies are urgently needed. The lack of animal models of AKI in the setting of advanced liver fibrosis hampers identification of the molecular drivers of AKI and this mouse model represents a unique opportunity to unveil the mechanisms involved in AKI associated with alcoholic fibrosis.

Our transcriptomic discoveries are most intriguing and provide important initial clues towards better characterization of the AKI pathology in alcoholic hepatitis. First, important linkages to the molecular signatures of alcoholic hepatitis in human liver were observed, such as marked upregulation of expression of osteopontin in a combined treatment group. Osteopontin, also known as secreted phosphoprotein 1 (*SPP1*), is an extracellular matrix

protein and a neutrophil-attracting chemokine; it is one of the most pronounced transcriptomic signals in liver in subjects with alcoholic hepatitis (Morales-Ibanez *et al.*, 2013). It is synthesized by multiple cell types and promotes profibrogenic and inflammatory actions through binding to integrins and CD44 (Wang and Denhardt, 2008). It plays role in a number of physiological and pathologic events such as cell adhesion, migration and cell survival, angiogenesis, apoptosis, inflammation and wound healing (Subraman *et al.*, 2015). Indeed, the immune response and activation of complement cascade and extracellular matrix-associated receptor activation and cytoskeleton remodeling pathways were among the most significant findings in the transcriptome analysis of the kidney effects of the combined treatment. This finding suggests that besides changes in vasoactive substances, an intrarenal inflammatory response, largely mediated by osteopontin and associated molecular drivers, could play a role in AKI in alcoholic cirrhosis. Further studies in humans should confirm this intriguing finding.

Another intriguing finding that points to a potential therapeutic intervention on the AKI component of alcoholic hepatitis is the PPARα pathway. PPARα agonists have been shown to be renoprotective (Wu *et al.*, 2009), including against renal fibrosis (Boor *et al.*, 2011). Renal fibrosis leads to downregulation of PPARα and mitigation of this effect with pharmacological agonists of this receptor is protective both in rats and *in vitro* (Boor *et al.*, 2011). We observed that PPARα associated pathways were not affected in kidney by CCl_4 and EtOH treatments individually, which may be one reason for the lack of injury and transcriptional response. However, major downregulation of PPARα-mediated fatty acid metabolism pathways in a combined treatment group was associated with pronounced nephropathy. It is well established that modulation of fatty acid and bile acid metabolism by PPARα agonists protects against alcoholic liver disease (Nakajima *et al.*, 2004; Li *et al.*, 2014) and thus it is likely that this protective effect may be also extendable to AKI phenotype in alcoholic hepatitis.

One important caveat to address in this model is the potential effects of CCl_4 and/or EtOH on Cyp2e1-mediated metabolism in the kidney. Co-administration of ETOH and CCl_4 affects pharmaco- and toxicokinetics of CCl_4 since both chemicals share Cyp2e1 as common metabolic pathway (Lieber, 1999). However, we posit that our data show that Cyp2e1 is unlikely to play a role in the observed kidney injury phenotype in this model. First, neither CCl_4 nor EtOH alone had an effect on Cyp2e1 protein in the kidney, even though a robust expected increase was observed in the liver of EtOH-treated mice. Second, circulating blood alcohol values are not affected by CCl_4. Finally, protein levels of Cyp2e1 were significantly down-regulated in the CCl_4(9w)+EtOH group, in both liver and kidney. Therefore, we reason that observed AKI and lipid peroxidation are due to inflammatory cell infiltration and other pathways, not through the Cyp2e1-mediated oxidative stress or metabolism of CCl_4 to reactive species.

In summary, we demonstrate that administration of alcohol in mice with severe liver fibrosis is associated with AKI. Transcriptomic analysis revealed that alcohol administration and fibrosis together have a multiplicative adverse effect on kidney function. This mouse model also exhibited similar pathological characteristics to human alcoholic hepatitis. Our findings reinforce the modern hypothesis that AKI in advanced liver disease is not merely a

consequence of systemic vasodilatation, but the response to systemic and intrarenal inflammation (Bernardi *et al.*, 2015). Recent clinical evidence shows that most patients with alcoholic hepatitis die due to multiorgan dysfunction and that AKI is by far the major accompanying organ failure (Michelena *et al.*, 2015). This clinical condition is without effective therapeutic options. Many patients with these complications do not respond to vasoconstrictors plus albumin. Likewise, renal replacement therapy is associated with high mortality rate. While it is likely that novel therapies for AKI will increase the survival of these patients, the development of new treatments is hampered by the poor knowledge of the mechanisms of AKI in this setting. Thus, identifying key molecular mechanisms of AKI in advanced alcoholic liver disease is the first step and an animal model of AKI in the setting of alcoholic cirrhosis, as detailed in this study, will be a useful research tool.

Supplementary Material

Refer to Web version on PubMed Central for supplementary material.

Acknowledgments

This work was funded, in part, by a grant from the National Institutes of Health (NIAAA, U01 AA021908).

References

Affo S, Morales-Ibanez O, Rodrigo-Torres D, Altamirano J, Blaya D, Dapito DH, Millan C, Coll M, Caviglia JM, Arroyo V, Caballeria J, Schwabe RF, Gines P, Bataller R, Sancho-Bru P. CCL20 mediates lipopolysaccharide induced liver injury and is a potential driver of inflammation and fibrosis in alcoholic hepatitis. Gut. 2014; 63:1782–1792. [PubMed: 24415562]

Altamirano J, Fagundes C, Dominguez M, Garcia E, Michelena J, Cardenas A, Guevara M, Pereira G, Torres-Vigil K, Arroyo V, Caballeria J, Gines P, Bataller R. Acute kidney injury is an early predictor of mortality for patients with alcoholic hepatitis. Clin Gastroenterol Hepatol. 2012; 10:65–71. [PubMed: 21946124]

Altamirano J, Miquel R, Katoonizadeh A, Abraldes JG, Duarte-Rojo A, Louvet A, Augustin S, Mookerjee RP, Michelena J, Smyrk TC, Buob D, Leteurtre E, Rincon D, Ruiz P, Garcia-Pagan JC, Guerrero-Marquez C, Jones PD, St Barritt A, Arroyo V, Bruguera M, Banares R, Gines P, Caballeria J, Roskams T, Nevens F, Jalan R, Mathurin P, Shah VH, Bataller R. A histologic scoring system for prognosis of patients with alcoholic hepatitis. Gastroenterology. 2014; 146:1231–1239. [PubMed: 24440674]

Belcher JM, Garcia-Tsao G, Sanyal AJ, Thiessen-Philbrook H, Peixoto AJ, Perazella MA, Ansari N, Lim J, Coca SG, Parikh CR, Consortium TA. Urinary biomarkers and progression of AKI in patients with cirrhosis. Clin J Am Soc Nephrol. 2014; 9:1857–1867. [PubMed: 25183658]

Bergmeyer, HU. Methods of enzymatic analysis. Academic Press; New York: 1988.

Bernardi M, Moreau R, Angeli P, Schnabl B, Arroyo V. Mechanisms of decompensation and organ failure in cirrhosis: From peripheral arterial vasodilation to systemic inflammation hypothesis. J Hepatol. 2015; 63:1272–1284. [PubMed: 26192220]

Bertola A, Mathews S, Ki SH, Wang H, Gao B. Mouse model of chronic and binge ethanol feeding (the NIAAA model). Nature Protocols. 2013; 8:627–637. [PubMed: 23449255]

Boor P, Celec P, Martin IV, Villa L, Hodosy J, Klenovicsova K, Esposito C, Schafer S, Albrecht-Kupper B, Ostendorf T, Heidland A, Sebekova K. The peroxisome proliferator-activated receptor-alpha agonist, BAY PP1, attenuates renal fibrosis in rats. Kidney Int. 2011; 80:1182–1197. [PubMed: 21814170]

Bradford BU, Kono H, Isayama F, Kosyk O, Wheeler MD, Akiyama TE, Bleye L, Krausz KW, Gonzalez FJ, Koop DR, Rusyn I. Cytochrome P450 CYP2E1, but not nicotinamide adenine

dinucleotide phosphate oxidase, is required for ethanol-induced oxidative DNA damage in rodent liver. Hepatology. 2005; 41:336–344. [PubMed: 15660387]

Cabre M, Camps J, Paternain JL, Ferre N, Joven J. Time-course of changes in hepatic lipid peroxidation and glutathione metabolism in rats with carbon tetrachloride-induced cirrhosis. Clin Exp Pharmacol Physiol. 2000; 27:694–699. [PubMed: 10972535]

Casanova J, Bataller R. Alcoholic hepatitis: Prognosis and treatment. Gastroenterol Hepatol. 2014; 37:262–268. [PubMed: 24656653]

Chiang DJ, Roychowdhury S, Bush K, McMullen MR, Pisano S, Niese K, Olman MA, Pritchard MT, Nagy LE. Adenosine 2A receptor antagonist prevented and reversed liver fibrosis in a mouse model of ethanol-exacerbated liver fibrosis. PLoS One. 2013; 8:e69114. [PubMed: 23874883]

Dennis G Jr, Sherman BT, Hosack DA, Yang J, Gao W, Lane HC, Lempicki RA. DAVID: Database for Annotation, Visualization, and Integrated Discovery. Genome Biol. 2003; 4:3.

Egerod Israelsen M, Gluud LL, Krag A. Acute kidney injury and hepatorenal syndrome in cirrhosis. J Gastroenterol Hepatol. 2015; 30:236–243. [PubMed: 25160511]

European Association for the Study of Liver. EASL clinical practical guidelines: management of alcoholic liver disease. J Hepatol. 2012; 57:399–420. [PubMed: 22633836]

French SW. The pathogenesis and significance of the urinary alcohol cycle in rats fed ethanol intragastrically. Alcohol Clin Exp Res. 2005; 29:158S–161S. [PubMed: 16344601]

Garcia-Tsao G, Parikh CR, Viola A. Acute kidney injury in cirrhosis. Hepatology. 2008; 48:2064–2077. [PubMed: 19003880]

Gines P, Schrier RW. Renal failure in cirrhosis. N Engl J Med. 2009; 361:1279–1290. [PubMed: 19776409]

Gomez-Hurtado I, Santacruz A, Peiro G, Zapater P, Gutierrez A, Perez-Mateo M, Sanz Y, Frances R. Gut microbiota dysbiosis is associated with inflammation and bacterial translocation in mice with CCl4-induced fibrosis. PLoS One. 2011; 6:e23037. [PubMed: 21829583]

Guan Y. Peroxisome proliferator-activated receptor family and its relationship to renal complications of the metabolic syndrome. J Am Soc Nephrol. 2004; 15:2801–2815. [PubMed: 15504933]

Humphreys BD, Lin SL, Kobayashi A, Hudson TE, Nowlin BT, Bonventre JV, Valerius MT, McMahon AP, Duffield JS. Fate tracing reveals the pericyte and not epithelial origin of myofibroblasts in kidney fibrosis. Am J Pathol. 2010; 176:85–97. [PubMed: 20008127]

Kisseleva T, Cong M, Paik Y, Scholten D, Jiang C, Benner C, Iwaisako K, Moore-Morris T, Scott B, Tsukamoto H, Evans SM, Dillmann W, Glass CK, Brenner DA. Myofibroblasts revert to an inactive phenotype during regression of liver fibrosis. Proc Natl Acad Sci U S A. 2012; 109:9448–9453. [PubMed: 22566629]

Kono H, Bradford BU, Rusyn I, Fujii H, Matsumoto Y, Yin M, Thurman RG. Development of an intragastric enteral model in the mouse: studies of alcohol-induced liver disease using knockout technology. J Hepatobiliary Pancreat Surg. 2000; 7:395–400. [PubMed: 11180860]

Latchoumycandane C, Nagy LE, McIntyre TM. Chronic ethanol ingestion induces oxidative kidney injury through taurine-inhibitable inflammation. Free Radic Biol Med. 2014; 69:403–416. [PubMed: 24412858]

Lauterburg BH, Velez ME. Glutathione deficiency in alcoholics: risk factor for paracetamol hepatotoxicity. Gut. 1988; 29:1153–1157. [PubMed: 3197987]

Li HH, Tyburski JB, Wang YW, Strawn S, Moon BH, Kallakury BV, Gonzalez FJ, Fornace AJ Jr. Modulation of fatty acid and bile acid metabolism by peroxisome proliferator-activated receptor alpha protects against alcoholic liver disease. Alcohol Clin Exp Res. 2014; 38:1520–1531. [PubMed: 24773203]

Lieber CS. Microsomal ethanol-oxidizing system (MEOS): the first 30 years (1968–1998)--a review. Alcohol Clin Exp Res. 1999; 23:991–1007. [PubMed: 10397283]

Lu SC, Tsukamoto H, Mato JM. Role of abnormal methionine metabolism in alcoholic liver injury. Alcohol. 2002; 27:155–162. [PubMed: 12163143]

Martin-Llahi M, Guevara M, Torre A, Fagundes C, Restuccia T, Gilabert R, Sola E, Pereira G, Marinelli M, Pavesi M, Fernandez J, Rodes J, Arroyo V, Gines P. Prognostic importance of the cause of renal failure in patients with cirrhosis. Gastroenterology. 2011; 140:488–496. e484. [PubMed: 20682324]

Melnyk S, Pogribna M, Pogribny I, Hine RJ, James SJ. A new HPLC method for the simultaneous determination of oxidized and reduced plasma aminothiols using coulometric electrochemical detection. J Nutr Biochem. 1999; 10:490–497. [PubMed: 15539328]

Michelena J, Altamirano J, Abraldes JG, Affo S, Morales-Ibanez O, Sancho-Bru P, Dominguez M, Garcia-Pagan JC, Fernandez J, Arroyo V, Gines P, Louvet A, Mathurin P, Mehal WZ, Caballeria J, Bataller R. Systemic inflammatory response and serum lipopolysaccharide levels predict multiple organ failure and death in alcoholic hepatitis. Hepatology. 2015; 62:762–772. [PubMed: 25761863]

Morales-Ibanez O, Dominguez M, Ki SH, Marcos M, Chaves JF, Nguyen-Khac E, Houchi H, Affo S, Sancho-Bru P, Altamirano J, Michelena J, Garcia-Pagan JC, Abraldes JG, Arroyo V, Caballeria J, Laso FJ, Gao B, Bataller R. Human and experimental evidence supporting a role for osteopontin in alcoholic hepatitis. Hepatology. 2013; 58:1742–1756. [PubMed: 23729174]

Naito Y, Bono H. GGRNA: an ultrafast, transcript-oriented search engine for genes and transcripts. Nucleic Acids Res. 2012; 40:W592–596. [PubMed: 22641850]

Nakajima T, Kamijo Y, Tanaka N, Sugiyama E, Tanaka E, Kiyosawa K, Fukushima Y, Peters JM, Gonzalez FJ, Aoyama T. Peroxisome proliferator-activated receptor alpha protects against alcohol-induced liver damage. Hepatology. 2004; 40:972–980. [PubMed: 15382117]

Niki E. Lipid peroxidation products as oxidative stress biomarkers. Biofactors. 2008; 34:171–180. [PubMed: 19706982]

Ogawa M, Mori T, Mori Y, Ueda S, Azemoto R, Makino Y, Wakashin Y, Ohto M, Wakashin M, Yoshida H, et al. Study on chronic renal injuries induced by carbon tetrachloride: selective inhibition of the nephrotoxicity by irradiation. Nephron. 1992; 60:68–73. [PubMed: 1738417]

Parola M, Pinzani M, Casini A, Leonarduzzi G, Marra F, Caligiuri A, Ceni E, Biondi P, Poli G, Dianzani MU. Induction of procollagen type I gene expression and synthesis in human hepatic stellate cells by 4-hydroxy-2,3-nonenal and other 4-hydroxy-2,3-alkenals is related to their molecular structure. Biochem Biophys Res Commun. 1996; 222:261–264. [PubMed: 8670193]

Powell CL, Bradford BU, Craig CP, Tsuchiya M, Uehara T, O'Connell TM, Pogribny IP, Melnyk S, Koop DR, Bleyle L, Threadgill DW, Rusyn I. Mechanism for prevention of alcohol-induced liver injury by dietary methyl donors. Toxicol Sci. 2010; 115:131–139. [PubMed: 20118189]

Rusyn I, Bataller R. Alcohol and toxicity. J Hepatol. 2013; 59:387–388. [PubMed: 23391479]

Sakhuja P. Pathology of alcoholic liver disease, can it be differentiated from nonalcoholic steatohepatitis? World J Gastroenterol. 2014; 20:16474–16479. [PubMed: 25469015]

Salerno F, Gerbes A, Gines P, Wong F, Arroyo V. Diagnosis, prevention and treatment of hepatorenal syndrome in cirrhosis. Gut. 2007; 56:1310–1318. [PubMed: 17389705]

Santos NA, Bezerra CS, Martins NM, Curti C, Bianchi ML, Santos AC. Hydroxyl radical scavenger ameliorates cisplatin-induced nephrotoxicity by preventing oxidative stress, redox state unbalance, impairment of energetic metabolism and apoptosis in rat kidney mitochondria. Cancer Chemother Pharmacol. 2008; 61:145–155. [PubMed: 17396264]

Schaeffner E, Ritz E. Alcohol and kidney damage: a Janus-faced relationship. Kidney Int. 2012; 81:816–818. [PubMed: 22377829]

Subraman V, Thiyagarajan M, Malathi N, Rajan ST. OPN -Revisited. J Clin Diagn Res. 2015; 9:ZE10–13.

Tsuchiya M, Ji C, Kosyk O, Shymonyak S, Melnyk S, Kono H, Tryndyak V, Muskhelishvili L, Pogribny IP, Kaplowitz N, Rusyn I. Interstrain differences in liver injury and one-carbon metabolism in alcohol-fed mice. Hepatology. 2012; 56:130–139. [PubMed: 22307928]

Uehara T, Ainslie GR, Kutanzi K, Pogribny IP, Muskhelishvili L, Izawa T, Yamate J, Kosyk O, Shymonyak S, Bradford BU, Boorman GA, Bataller R, Rusyn I. Molecular mechanisms of fibrosis-associated promotion of liver carcinogenesis. Toxicol Sci. 2013; 132:53–63. [PubMed: 23288052]

Uehara T, Pogribny IP, Rusyn I. The DEN and CCl4 -Induced Mouse Model of Fibrosis and Inflammation-Associated Hepatocellular Carcinoma. Curr Protoc Pharmacol. 2014; 66:14 30 10. [PubMed: 25181010]

Ueno A, Lazaro R, Wang PY, Higashiyama R, Machida K, Tsukamoto H. Mouse intragastric infusion (iG) model. Nature Protocols. 2012; 7:771–781. [PubMed: 22461066]

Van Thiel DH, Gavaler JS, Little JM, Lester R. Alcohol: its effect on the kidney. Adv Exp Med Biol. 1977; 85A:449–457. [PubMed: 920491]

Wang KX, Denhardt DT. Osteopontin: role in immune regulation and stress responses. Cytokine Growth Factor Rev. 2008; 19:333–345. [PubMed: 18952487]

Weiler-Normann C, Herkel J, Lohse AW. Mouse models of liver fibrosis. Z Gastroenterol. 2007; 45:43–50. [PubMed: 17236120]

World Health Organization. Global status report on alcohol and health. WHO Press; Geneva, Switzerland: 2014.

Wu J, Chen L, Zhang D, Huo M, Zhang X, Pu D, Guan Y. Peroxisome proliferator-activated receptors and renal diseases. Front Biosci (Landmark Ed). 2009; 14:995–1009. [PubMed: 19273113]

Zakhari S. Overview: how is alcohol metabolized by the body? Alcohol Res Health. 2006; 29:245–254. [PubMed: 17718403]

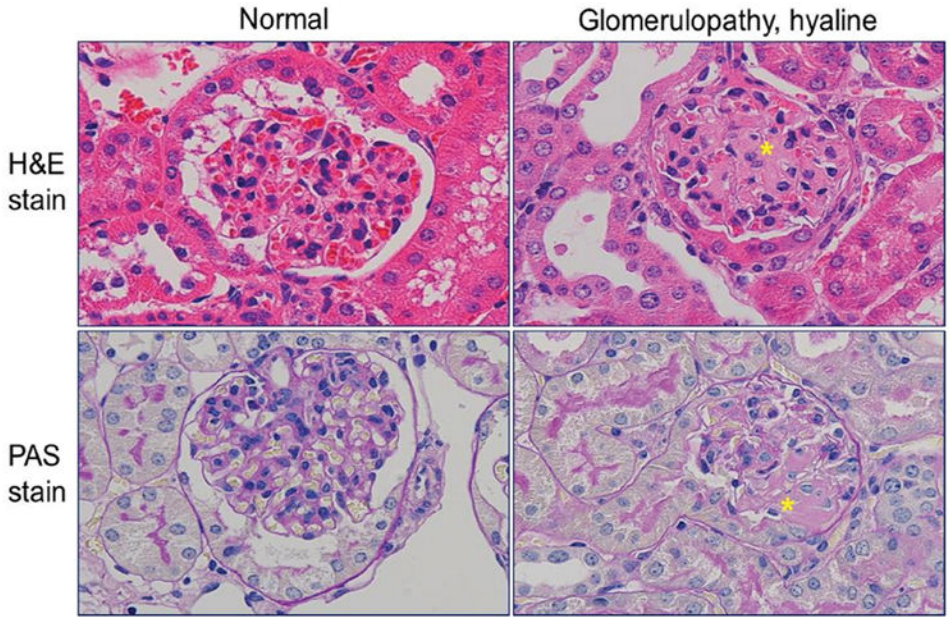

Figure 1.

Representative photomicrographs of kidney sections from two different male C57BL/6J mice treated with alcohol (up to 27 g/kg/day) intragastrically for 28 days [animal treatments are detailed in (Tsuchiya et al., 2012)]. Left panel, one representative animal without kidney injury; right panel, one representative animal with mild hyaline glomerulopathy (star indicated affected glomerulus). Top row, images of H&E; bottom row, PAS staining. Original magnification, 200×.

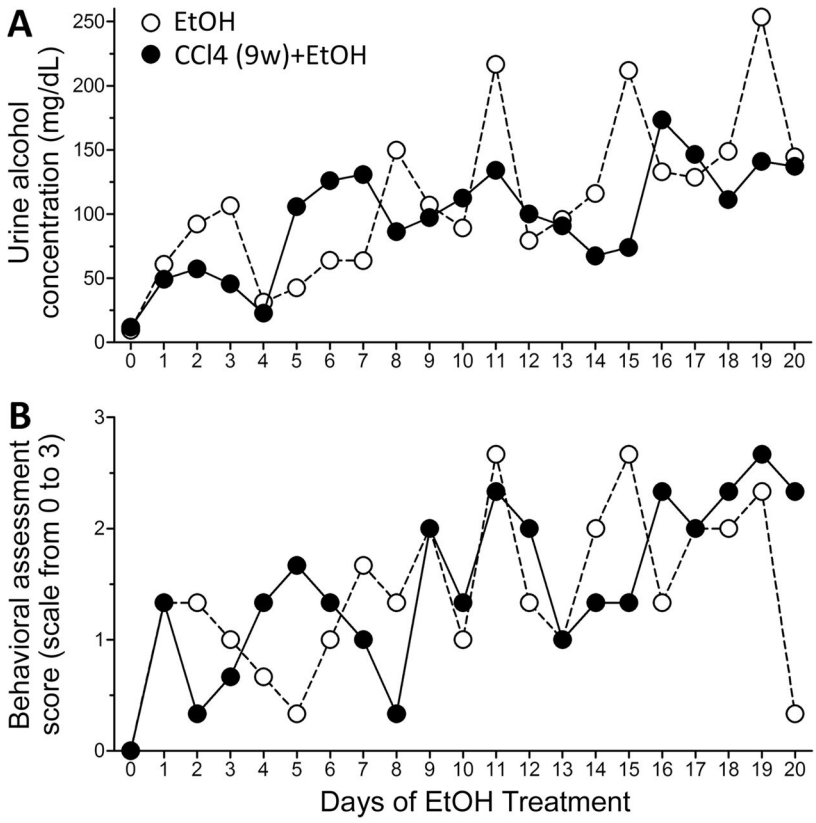

Figure 2.

Daily average urine alcohol concentrations (A) and behavioral scores (B) in mice treated with alcohol intragastrically (EtOH, open circles) or with CCl_4 and alcohol (CCl_4(9w) +EtOH, filled circles) as detailed in Methods and Supplemental Figure 1.

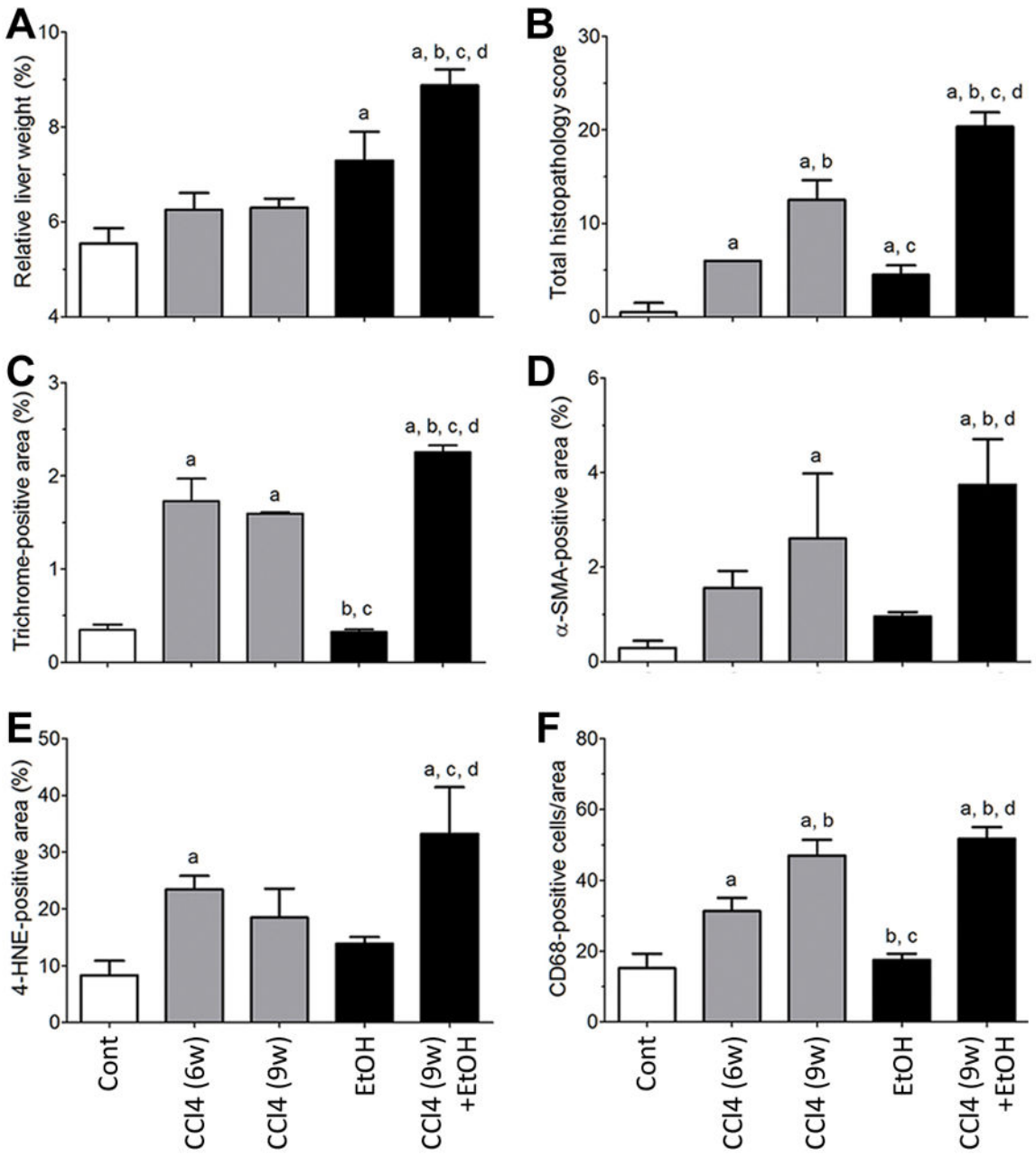

Figure 3.

Quantitative analysis of liver injury phenotypes. (A) Relative liver weight (%) to body weight. (B) Total liver histopathological score as evaluated in a blind test by two certified veterinary pathologists. Quantitative analysis of staining for Masson's trichrome (C), α-SMA (D), or 4-HNE (E) in liver sections was expressed as % of positive staining area relative to total area in five random at 200× magnification fields. (F) Quantitative analysis of CD68-positive cells was expressed as an average number of stained cells in five random fields at 200× magnification. All data are presented as mean±SD. $^{a}p< 0.05$, compared to control group; $^{b}p< 0.05$, compared to CCl_4 (6w) group; $^{c}p< 0.05$, compared to CCl_4 (9w) group; $^{d}p< 0.05$, compared to the alcohol alone (EtOH) group.

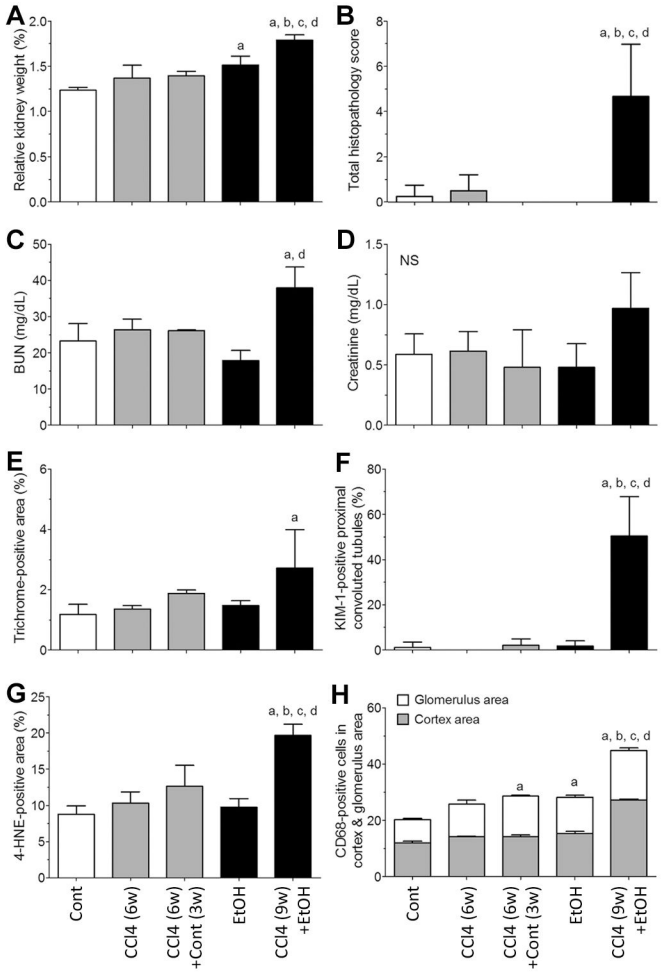

Figure 4.

Quantitative analysis of kidney injury phenotypes. (A) Relative kidney weight (%) to body weight. Blood urea nitrogen (BUN, B) and serum creatinine (C) levels, as measured by an enzymatic assay. (D) Total kidney histopathological score, as evaluated in a blind test by two certified veterinary pathologists. Quantitative analysis of staining for Masson's trichrome (E), α-SMA (F), or 4-HNE (G) in liver sections was expressed as % of positive staining area relative to total area in five random at 200× magnification fields. (H) Quantitative analysis of CD68-positive cells was expressed as an average number of stained cells in five random fields at 200× magnification. Cell counting was performed separately for the glomeruli (white bars) and cortex (gray bars). All data are presented as mean±SD. Asterisks indicate significant differences among groups as indicated in the legend to Figure 3.

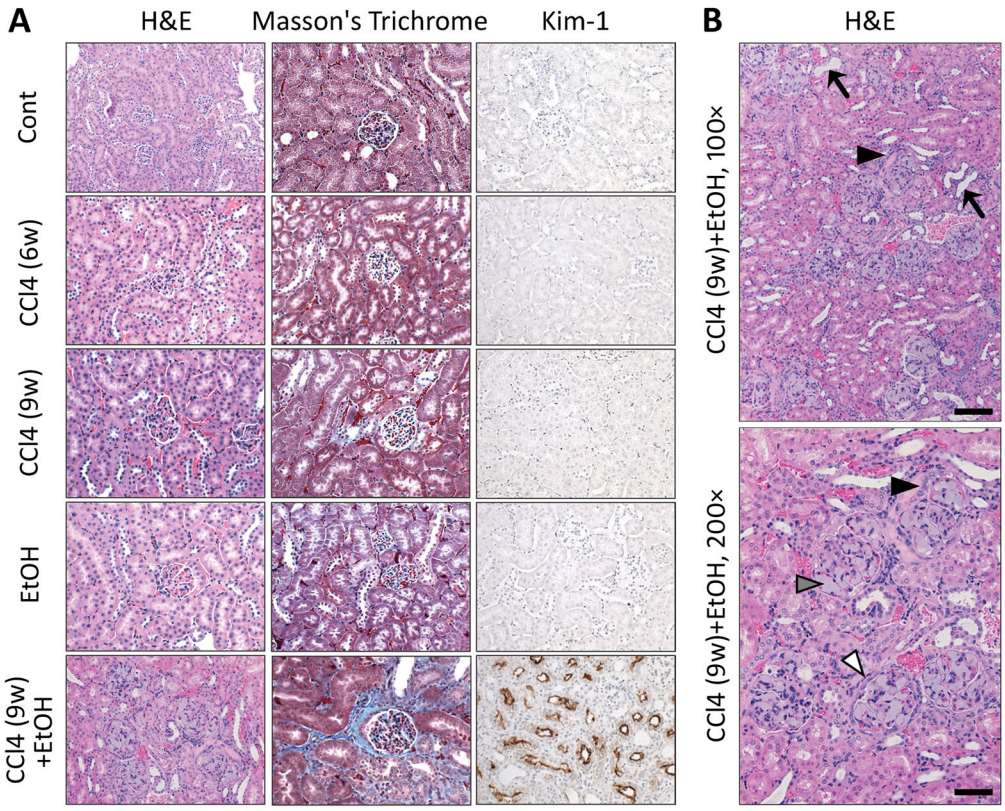

Figure 5.

Representative photomicrographs of kidney sections from Control, CCl_4(6w), CCl_4(9w), EtOH and CCl_4(9w)+EtOH groups. (A) Images of H&E (left) and Masson's trichrome (middle) staining, as well as immunostaining for kidney injury molecule-1 (Kim-1, right). Original magnification, 200×. Scale bar, 100μm. (B) H&E-stained sections of kidney tissue from CCl_4(9w)+EtOH group. Top, original magnification, 100×, scale bar, 200μm. Arrows point to dilated renal tubules. Black arrowhead points to the regenerating renal tubules. Bottom, original magnification, 200×, scale bar, 100μm. Gray arrowhead points to the area of amphophilic material deposition in the glomerulus; white arrowhead points to the fibrosis capsule of the glomerulus.

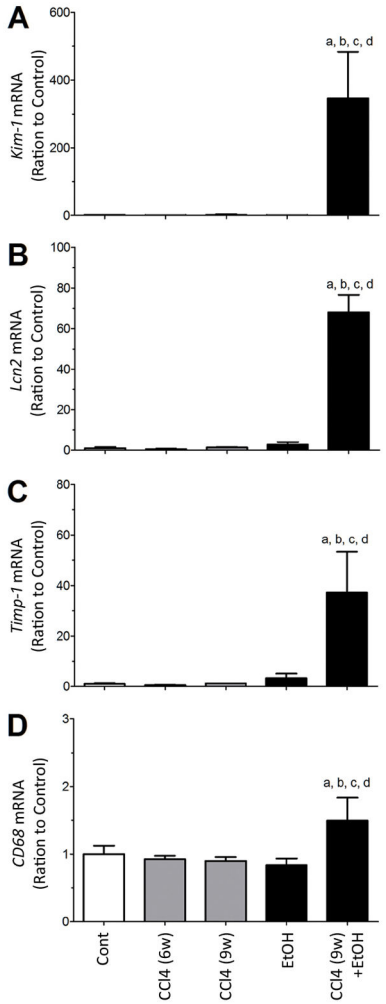

Figure 6.

Quantitative analysis of kidney injury markers performed by qRT-PCR. (A) *Kim-1*; Biomarker for renal proximal tubule injury. (B) *Lcn2*; one of the biomarker of acute kidney injury (AKI). (C) *Timp-1*; fibrosis marker. (D) *CD68*; general macrophage marker of inflammation. All data are presented as mean±SD. Asterisks indicate significant differences among groups as indicated in the legend to Figure 3.

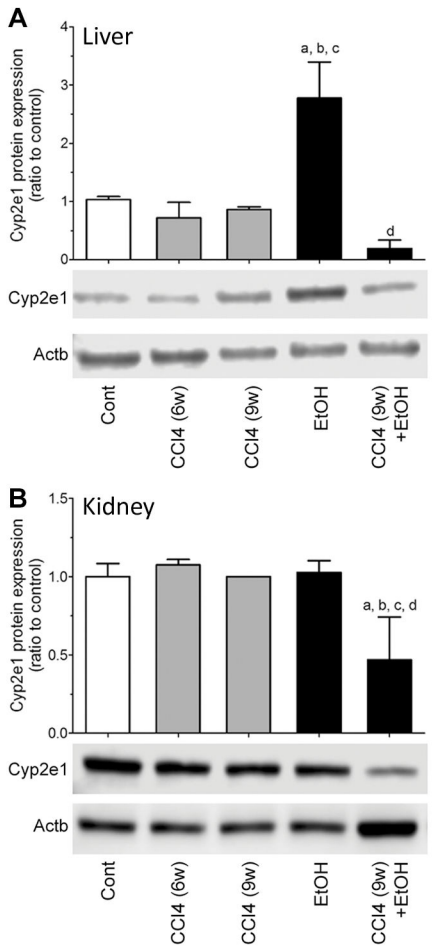

Figure 7.

Quantitative analysis of Cyp2e1 protein level in liver (A), and kidney (B). All data are presented as mean±SD. Asterisks indicate significant differences among groups as indicated in the legend to Figure 3. Representative images of the Western blots are shown below each bar chart. Protein level of Cyp2e1 and β-actin (Actb) is shown for one sample from each group.

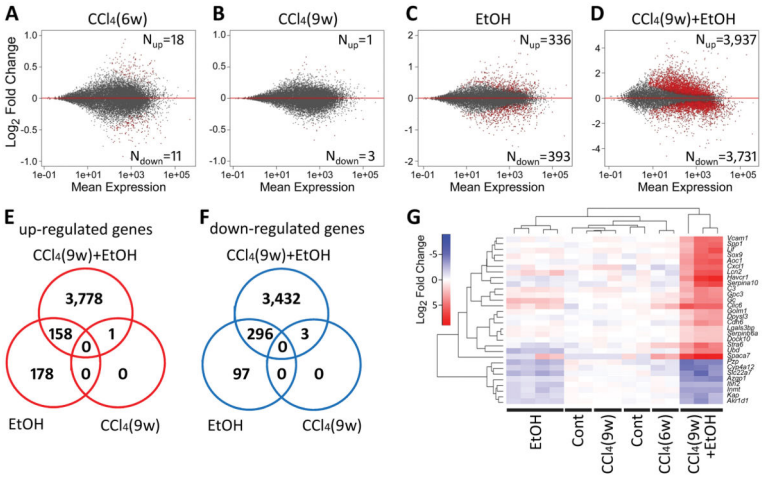

Figure 8.

Transcriptional effects in mouse kidney. (A–D) Scatter plots of gene expression changes, relative to control group, upon treatment with (A) CCl_4(6w), (B) CCl_4(9w), (C) EtOH, or (D) CCl_4(9w)+EtOH. Red dots indicate significant ($q<0.1$) differentially expressed genes. (E–F) Venn diagrams of significant differentially expressed (E, for up-regulated; F, for down-regulated) genes among CCl_4(9w), EtOH, and CCl_4(9w)+EtOH groups. (G) Heat map of 30 most significant differentially expressed genes (see Supplemental Table 3 for a complete ranked list). Colors indicate the fold change in expression difference from the mean of control samples, transformed to log2 ratios (see color bar). Samples and transcripts are clustered by correlation as indicated by the dendrograms. Group assignment of each sample is indicated at the bottom of the figure.

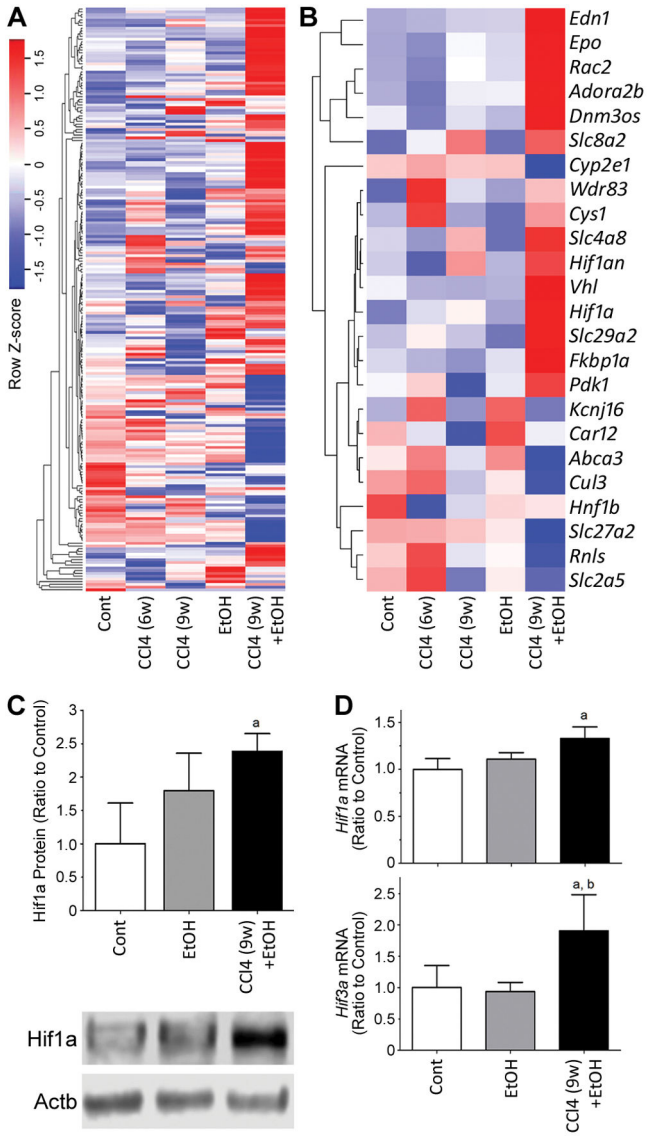

Figure 9.

Hypoxia-associated effects in a mouse model of alcoholic liver fibrosis-associated acute kidney injury. Supervised clustering diagrams of 213 (panel A, the ranked list of transcripts in this figure is included in Supplemental Table 4) and 24 (panel B and Supplemental Table 4) transcripts identified as related to hypoxia in general, or hypoxia and kidney, respectively, in GGRNA (Naito and Bono, 2012). Colors indicate the fold change in expression difference from the mean of control samples, transformed to Z-score for each row (see color bar in panel A). Quantitative analysis of kidney levels of Hif1a protein (C), and *Hif1a* and *Hif3a* mRNA (D). All data are presented as mean±SD. Asterisks indicate significant differences among groups as indicated in the legend to Figure 3. Representative images of the Western blots are shown below bar chart in C. Protein level of Hif1a and β-actin (Actb) is shown for one sample from each group.